Spin, charge, and orbital orderings in oxides with dual-valent transition metal ions

R. Vidya*, P. Ravindran, P. Vajeeston, H. Fjellvåg, A. Kjekshus

Department of Chemistry, University of Oslo, Box 1033 Blindern, N-0315 Oslo, Norway

Abstract

Using generalized-gradient-corrected full-potential density-functional calculations, we have studied the electronic structure and magnetic properties of $YBaMn_2O_5$, $Sr_4Fe_4O_{11}$, and $Ca_3Co_2O_6$. In these phases, the $3d$ transition metal ions have dual valence. We have studied the electronic structure using site-, angular momentum-, and orbital-projected density of states. The charge and orbital ordering are analyzed in terms of the calculated electron-density distribution, charge density, and electron localization function. The oxygen vacancy, cation radii, and crystal-field effects are found to play an important role for the various ordering phenomena in these compounds.
© 2004 Elsevier Ltd and Techna Group S.r.l. All rights reserved.

Keywords: C. Magnetic properties; D. Transition metal oxides; Spin, charge, and orbital ordering

1. Introduction

Since the discovery of colossal magnetoresistance (CMR) in perovskite-like manganites there have been increased activities on related oxides with dual-valent transition metal constituents. Beside the technological interest in the CMR effect, other related phenomena (attractive from more fundamental points of view) have been established for dual-valent compounds. A very interesting phenomenon is the tendency displayed by many transition metal oxides to adopt the kind of charge distribution known as charge ordering (CO). Although covalence effects in such compounds can be significant, the ionic picture describes it as a real-space ordering of charges and/or orbitals. In general, the Coulomb repulsion between the charges and the elastic energy perturbation owing to cooperative Jahn–Teller (JT) distortions favor the CO. Large radius of (what may be conveniently named) A-site cations (R_A) and wide e_g bandwidths, favor the mobility of the electrons through the lattice, while smaller R_A and narrow e_g bandwidths, favor localization [1]. CO is interesting because double-exchange gives rise to metallicity along with ferromagnetism (F) while the CO state can be associated with insulating and antiferromagnetic (AF) behavior. Hence, there is a competition between F with metallic behavior and insulating AF character with CO. Orbital ordering (OO) gives rise to anisotropic interactions in the electron-transfer process which in turn favor or disfavor the double- and super-exchange (F or AF) interactions in an orbital direction-dependent manner. Understanding of the CO, OO, and spin ordering (SO) processes, provides a foundation for deeper penetration into the complex behaviors of CMR materials.

In the present work, we analyze the spin, charge, and orbital orderings present in the dual-valent oxides (with crystal structure more or less related to the perovskite-type) $YBaMn_2O_5$ (YBMO), $Sr_4Fe_4O_{11}$ (SFO), and $Ca_3Co_2O_6$ (CCO). We have used full-potential density-functional calculations to understand the electronic and magnetic properties and the various orderings present in these phases.

2. Computational details

The full-potential linear muffin-tin orbital (FPLMTO) calculations [2] presented in this paper are all-electron, and no shape approximation to the charge density or potential has been used. The basis set is comprised of augmented linear muffin-tin orbitals [3]. The calculations

---

* Corresponding author.
E-mail address: vidya.ravindran@kjemi.uio.no (R. Vidya).
URL: http://folk.uio.no/ravindrv.

are based on the generalized-gradient-corrected (GGA) density-functional theory as proposed by Perdew et al. [4]. Spin–orbit coupling is included directly in the Hamiltonian matrix elements for the part inside the muffin-tin spheres, hence for spin-polarized cases the size of the secular matrix is doubled. We used a multi-basis in order to ensure well-converged wave functions. This means that several Hankel or Neumann functions, each attached to its own radial function, have been used. The basis included are Y $4p$, $5s$, $5p$, and $4d$, Ba $5p$, $6s$, $6p$, $5d$, and $4f$, Mn $4s$, $4p$, and $3d$, and O $2s$, $2p$, and $3d$ for YBMO, Sr $5s$, $4p$, $4d$, and $4f$, as well as pseudo-core $5p$, Fe $4s$, $4p$, and $3d$, and O $2s$, $2p$, and $3d$ for SFO, and Ca $4s$, $4p$, and $3d$, Co $4s$, $4p$, and $3d$, and O $2s$, $2p$, and $3d$ for CCO. For the total-energy study the $\boldsymbol{k}$-space integration is done with 192, 144, and 90 $\boldsymbol{k}$ points for YBMO, SFO, and CCO, respectively, in the irreducible part of the first Brillouin zone. For the magnetic calculations, the easy magnetization axis is chosen in accordance with experimental findings [5–7].

3. Results and discussion

3.1. YBaMn$_2$O$_5$

The ordered oxygen-deficient double perovskites RBaT_2O$_5$ (R = rare-earth and T = Mn, Fe, or Co) have attracted much attention as new spin–charge–orbital coupled CMR materials. CMR effects of some 40% are observed in the isostructural phases with R = Gd or Eu [8]. At low temperature, YBMO is an AF insulator with CO of Mn^{3+} and Mn^{2+} accompanied by OO and SO. The crystal structure (Fig. 1) is described in the space group $P4/nmm$ with two kinds of MnO$_5$ pyramids arranged in an ordered manner, each Mn^{2+}O$_5$ pyramid being linked to five Mn^{3+}O$_5$ pyramids and vice versa [5]. Oxygen takes two crystallographically different sites with O(1) at the base of the square pyramids, and O(2) at the apex. The basal plane Mn^{3+}–O(1)–Mn^{2+} angle is 157.8° and the apical Mn^{3+}–O(2)–Mn^{2+} angle is 180°. The large difference in these angles play a key role in the magnetic properties.

Table 1
Calculated magnetic moment (in μ_B per T atom at 0 K) for YBMO, SFO, and CCO in the ground-state configuration

Compound	Theory			Experiment		
	T(1)	T(2)	Total	T(1)	T(2)	Total
YBaMn$_2$O$_5$ (YBMO)	3.07	3.93	0.86	2.91	3.91	0.95
Sr$_4$Fe$_4$O$_{11}$ (SFO)	2.86	3.35	0.00	0.00	3.00	0.0
Ca$_3$Co$_2$O$_6$ (CCO)	0.17	2.63	1.21	0.08	3.00	1.3

Total refers to the total magnetic moment per formula unit. The experimental values are taken from Refs. [5–7].

Among the paramagnetic (P), F, and AF configurations considered for calculations [9], AF is found to have the lowest total energy. The ferromagnetic configuration is 505 meV/f.u. higher in energy than the AF configuration. Table 1 shows that the total magnetic moment is not completely canceled, resulting in a ferrimagnetic (Ferri) state. Mn(1) has a smaller magnetic moment (3.07 μ_B) than Mn(2) (3.91 μ_B) implying that Mn(1) corresponds to Mn^{3+} and Mn(2) to Mn^{2+}, both in high-spin states. The electronic structure indicates that it is an indirect band-gap semiconductor with a band gap of 0.88 eV, in agreement with experimental findings [10,11].

CO is expected to be favored when equal proportions of Mn^{2+} and Mn^{3+} are present like in YBMO. On reduction of the Mn–O–Mn angle, the hopping between the Mn $3d$ and O $2p$ orbitals decreases and hence the e_g bandwidth decreases. Consequently the system stabilizes in a Ferri-CO-insulating state. In order to visualize the presence of CO and Ferri SO in YBMO we show the calculated d-electron-density distribution for the Mn ions in the up- and down-spin channels in Fig. 1a and b. The CO in YBMO is characterized by the real-space ordering of Mn^{2+} and Mn^{3+}. The significant difference in the electron-density distribution for the Mn ions clearly indicates that there occurs two different valence states with different orbital occupation. This feature ensures that the spins do not cancel exactly, resulting in the Ferri ordering (Fig. 1c).

The exchange interaction between Mn^{2+} and Mn^{3+} along c is AF owing to the 180° bond angle which facilitates p–d σ bonding with the O(2) p_z orbital as well

Fig. 1. The calculated Mn d-electron-density distribution of (a) up- and (b) down-spin electrons in YBaMn$_2$O$_5$. (c) The G-type ferrimagnetic spin ordering and (d) orbital ordering in YBaMn$_2$O$_5$.

as super-exchange interaction [12]. With a bond angle of only 157° within the basal plane, the d(Mn)–p(O) covalent bond is weak and moreover due to the HS state of Mn^{3+} in the square-pyramidal crystal field, the $d_{x^2-y^2}$ orbital at the Mn^{3+} site is almost empty whereas that at Mn^{2+} is half filled. Hence, the AF super-exchange interaction between Mn^{2+} and Mn^{3+} within the basal plane is weaker than that along c.

In order to visualize the OO in YBMO we show in Fig. 1d the electrons distribution at the Mn sites between $-1\,eV$ and E_F (viz. the electrons mainly participating in the hopping interactions). In the bc plane the d_{z^2} orbital is ordered along c for both Mn^{3+} and Mn^{2+}, and this orbital hybridizes with the O(1) p_z orbital resulting in σ bonding. There is virtually no overlap between the $d_{x^2-y^2}$ and p_z orbitals because of their different orientation in the c direction. Therefore, the electron in the $d_{x^2-y^2}$ orbital can not hop along c. Moreover, the direct overlap between O $p_{x,y}$ and Mn d is small in the ab plane ($d_{x^2-y^2}$ is almost empty for Mn^{3+} and only partly occupied for Mn^{2+} due to the JT distortion) and hence the d electrons become localized resulting in CO and OO.

3.2. $Sr_4Fe_4O_{11}$

SFO is also an oxygen-deficient perovskite-like material which crystallizes in the space group $Cmmm$ [13]. It is an antiferromagnet with $T_N \approx 230\,K$. Fe has square-pyramidal [Fe(1)] and octahedral [Fe(2)] coordination polyhedra. Owing to the oxygen vacancy in the structure and different crystal-field effects Fe takes the dual-valent states Fe^{3+} and Fe^{4+}.

According to powder neutron diffraction data (at 8 K) this compound has an unusual magnetic structure; Fe(1) do not exhibit any magnetic ordering whereas Fe(2) ions have a G-type AF arrangement [7]. The room-temperature Mössbauer spectrum is reported [14] to show two symmetrical doublets of equal intensity. From the isomer-shift values (0.35 and $-0.08\,mm\,s^{-1}$) the two components are assigned to Fe^{3+} and Fe^{4+}. A hyperfine splitting and low flux density value has been observed for the Fe^{3+} component, whereas only a linewidth broadening is observed for the Fe^{4+} component below T_N. This suggests a partially frustrated AF structure [14]. Furthermore, a strong divergence between zero-field-cooled and field-cooled magnetic susceptibility curves is observed, implying spin-glass-like behavior [15].

We have carried out density-functional calculations in F as well as A-, C-, and G-type AF configurations and found that G-AF has the lowest energy. C-AF is the next stable state with 2.54 eV higher energy than the G-AF state. Our calculations show that G-AF configuration with zero magnetic moment for Fe(1) is higher in energy (1.85 eV) than that with a magnetic moment of $2.8\,\mu_B$ for Fe(1), indicating that the former may represent a meta-stable state. However, we have not considered temperature effects and oxygen vacancy ordering in our calculations which may play important roles for the magnetic properties. The unusual magnetic properties of SFO can be related to the crystal structure and the CO of the Fe ions. In order to be able to draw a more firm conclusion regarding the magnetic structure, further calculations including structural optimization is in progress.

A correct assignment of valence states to the Fe ions is essential to understand the relationship between the crystal structure and the electronic and magnetic properties. The Mössbauer studies appear to point to the presence of Fe^{3+} and Fe^{4+} ions. Crystal-field stabilization energy and the relative values of the bond-strength sums [13] indicate that Fe^{4+} should be assigned to square-pyramidal and Fe^{3+} to octahedral coordinations. If Fe(1) were an Fe^{4+} ion, it should be either in an intermediate-spin (IS; $t_{2g}^4 e_g^0$; $2\,\mu_B$) state or in a low-spin (LS; $t_{2g}^4 e_g^0$; $0\,\mu_B$) state. The octahedral Fe(2) should be Fe^{3+} in IS ($t_{2g}^4 e_g^1$; $3\,\mu_B$). An IS state for Fe(2) agrees very well with the theoretical and experimental magnetic moment and is consistent with the JT distortion observed.

The electronic structure of SFO in the G-AF state is consistent with metallic conductivity with a low density of states (DOS) at the Fermi level (E_F). The partial DOS analysis shows that the Fe $3d$ and O $2p$ states are energetically degenerate leading to covalent interaction between them. However, as the topology of the DOS curves for Fe(1) and Fe(2) is different (Fig. 2), the magnitude of the covalent interaction is also different. In the G-AF state with the zero magnetic moment for Fe(1), the up- and down-spin DOS of Fe(1) are similar, implying that the up- and down-spin channels have the same occupancy, viz. complying with the zero magnetic moment. This emphasizes the fact that Fe(1) exists in an Fe^{4+} LS state. The majority spin channel of Fe(2) has more states than the minority spin channel, giving a finite magnetic moment (also seen for Fe(1) in the G-AF situation where Fe(1) takes a finite magnetic moment). As the Fe(2)–O bond length (2.04 Å) is longer than the Fe(1)–O bond length (1.85 Å), the Fe(2)–O bond strength is weaker than that of Fe(1)–O. On the other hand, more unpaired $3d$ states are localized on Fe(2) than on Fe(1). Moreover, as the Fe(1)–O–Fe(2) bond angle is less than 180°, the super-exchange interaction is incomplete like the Mn(1)–O–Mn(2) super-exchange interaction in YBMO. These features lead to the CO in addition to the SO in SFO.

3.3. $Ca_3Co_2O_6$

CCO belongs to the family of one-dimensional (1-D) oxides. Inorganic structures with 1-D atomic arrangements are in the limelight owing to their unique electronic and magnetic properties [16]. The crystal structure of CCO consists of parallel 1-D Co–O chains separated by Ca^{2+} ions. The chains are built by alternating face-sharing CoO_6 octahedra and trigonal prisms along the hexagonal c axis. The resulting short metal–metal intrachain distance (2.59 Å) (compared to the interchain distance of 5.24 Å) reinforces the 1-D character of the structure along the c axis. Mag-
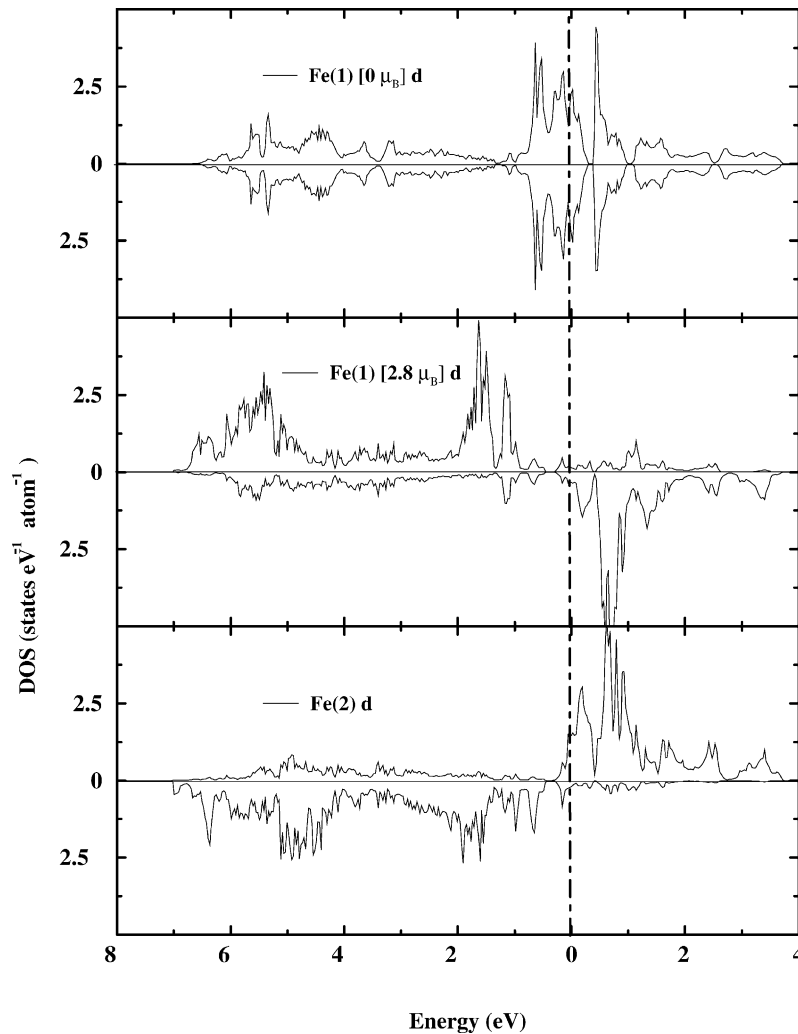
Fig. 2. The site- and angular momentum-projected density of states for Fe(1) and Fe(2) of $Sr_4Fe_4O_{11}$. The s and p partial DOSs are only about 10% of the d states shown.

netic studies show F intrachain ordering ($T_{C1} = 24$ K) with AF interchain coupling ($T_{C2} = 10$ K) [6]. For every two F-aligned Co chains, there is one AF-aligned chain giving a resultant Ferri structure.

Our total-energy study [17] shows that Ferri state of CCO has the lowest energy in perfect agreement with experimental findings [6,18]. The Ferri state is 114 meV/f.u. lower in energy than the F state. The electronic structure shows [17] a finite DOS at E_F in both spin channels, implying a metallic character consistent with the experimental conductivity study [19]. Our partial DOS analysis shows that the states in the vicinity of E_F are mainly contributed by Co d states.

Different spin configurations for the crystallographically different Co ions are expected [20] as a consequence of the larger crystal field for the octahedral Co(1) than for the trigonal prismatic Co(2). Various proposals have been made for spin states of Co such as (i) Co(1): LS Co^{3+}; Co(2): HS Co^{3+}, (ii) Co(1): LS Co^{4+}; Co(2): HS Co^{2+}, and (iii) Co(1): LS Co^{2+} and Co^{4+}; Co(2): HS Co^{3+}. The calcu-

lated magnetic moments listed in Table 1 are found to be in good agreement with available low-temperature neutron diffraction and magnetization data. By taking the magnetic moments at the Co sites into consideration, together with the octahedral and trigonal-prismatic crystal fields and the calculated site- and orbital-projected DOS features, we conclude that Co(1) is Co^{4+} in LS (d^5; $t_{2g}^5 e_g^0$) state and Co(2) is Co^{2+} in HS (d^7; $t_{2g}^5 e_g^2$) state.

As the interatomic distance in metallic Co is 2.51 Å and the distance between Co(1) and Co(2) in CCO is 2.59 Å, a metallic interaction between Co(1) and Co(2) has been anticipated [21]. However, our charge density and electron-localization-function analyses show very weak metallic interaction between the Co atoms. Moreover as seen from Fig. 3, the topology of DOS curves for Co(1) and Co(2) are entirely different implying differences in their valence and spin states. As the O $2p$ states are energetically degenerate with Co $3d$ states, there is strong covalent
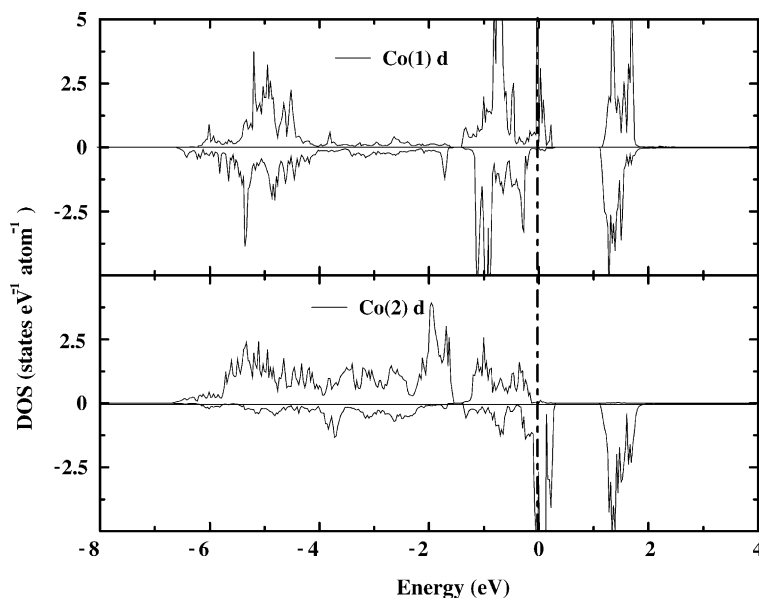
Fig. 3. The site- and angular momentum-projected density of states for Co(1) and Co(2) of $Ca_3Co_2O_6$. The Co s and p partial DOSs are only about 10% of the d states shown.

interaction between Co and O. However, the magnitude of covalent interaction is different for Co(1) and Co(2) owing to the difference in their crystal fields. Therefore, the localization of charges on Co(1) and Co(2) is different and leads to the ladder-type CO. Moreover, the orbital-projected DOS features show that both e_g and t_{2g} (except d_{xz}) orbitals have finite states close to E_F for Co(1) whereas only d_{xz} and d_{yz} orbitals have finite DOS in the same region for Co(2). Therefore, also the occupation of the d orbitals of Co(1) and Co(2) is different resulting in OO in addition to the CO and Ferri-SO situation.

4. Conclusions

We have studied the electronic and magnetic properties (in particular spin, charge, and orbital orderings) of YBMO, SFO, and CCO, using full-potential density-functional calculations. All the studied compounds have dual-valent transition metal ions which (together with at least two crystallographically non-equivalent T-atom sites) is a prerequisite for the ordering phenomena under investigation. The present study, however, shows that the phenomena are not connected to *one particular* structure type. In general, when the e_g bandwidth (determined mainly by the constituents of the compound) is small, charge ordering is favored. In YBMO, the distinction between the radii of Y and Ba together with oxygen vacancies (not discussed here) lead to difference in $T(1)$–O–$T(2)$ bond angles as well as T–O bond lengths. Hence the $T(1)$–O–$T(2)$ super-exchange interaction is not uniform in YBMO resulting in a charge ordering pattern of the checker-board type. Similarly, in SFO and CCO also the variation in the bond angles and bond lengths leads to difference in the valence states of the T ions and charge

ordering. The occupancy of the d orbitals and hence orbital ordering is determined by the coordination polyhedra surrounding the T ions. Therefore, the crystal-field effect and hence crystal structure of a compound play an important role in orbital ordering. All in all, the constituents of a given compound, the crystal structure (including crystal-field effects), and oxygen stoichiometry determine spin, charge, and orbital orderings in this type of materials. A study of the individual effect of the just mentioned ruling parameters may reveal more insight into the ordering phenomena.

Acknowledgements

References

[1] C.N.R. Rao, A.K. Raychaudhuri, in: C.N.R. Rao, B. Raveau (Eds.), Colossal Magnetoresistance, Charge Ordering and Related Properties of Manganese Oxides, World Scientific, Singapore, 1998, p. 31.

[2] J.M. Wills, O. Eriksson, M. Alouani, D.L. Price, in: H. Dreysse (Ed.), Electronic Structure and Physical Properties of Materials, Springer, Berlin, 2000, p. 148.

[3] O.K. Andersen, Phys. Rev. B 12 (1975) 3060.

[4] J.P. Perdew, K. Burke, M. Ernzerhof, Phys. Rev. Lett. 77 (1996) 3865.

[5] F. Millange, E. Suard, V. Caignaert, B. Raveau, Mater. Res. Bull. 34 (1999) 1.

[6] S. Aasland, H. Fjellvåg, B.C. Hauback, Solid State Commun. 101 (1997) 187.

[7] H. Fjellvåg, unpublished.

[8] C. Martin, A. Maignan, D. Pelloquin, N. Nguyen, B. Raveau, Appl. Phys. Lett. 71 (1997) 1421.

[9] R. Vidya, P. Ravindran, A. Kjekshus, H. Fjellvåg, Phys. Rev. B 65 (2002) 144422.

[10] J.P. Chapman, J.P. Attfield, M. Mölgg, C.M. Friend, T.M. Beales, Angew. Chem. Int. Ed. Engl. 35 (1996) 2482.

[11] T.P. Beales, M. Mölgg, J. Jutson, C.M. Friend, Phys. Stat. Sol. (A) 161 (1997) 271.

[12] J.B. Goodenough, Magnetism and the Chemical Bond, Wiley, New York, 1963.

[13] J.P. Hodges, S. Short, J.D. Jorgensen, X. Xiong, B. Dabrowski, S.M. Mini, C.W. Kimball, J. Solid State Chem. 151 (2000) 190.

[14] L. Fournes, Y. Potin, J.-C. Grenier, G. Damazeau, M. Pouchard, Solid State Commun. 62 (1987) 239.

[15] T.C. Gibb, J. Chem. Soc., Dalton Trans. (1985) 1455.

[16] T.N. Nguyen, H.-C. zur Loye, J. Solid State Chem. 117 (1995) 300.

[17] R. Vidya, P. Ravindran, H. Fjellvåg, A. Kjekshus, O. Eriksson, Phys. Rev. Lett. 91 (2003) 186404.

[18] H. Kageyama, K. Yoshimura, K. Kosuge, X. Xu, S. Kawano, J. Phys. Soc. Jpn. 67 (1998) 357.

[19] A. Maignan, C. Michel, A.C. Masset, C. Martin, B. Raveau, Eur. Phys. J. B 15 (2000) 657.

[20] H. Kageyama, K. Yoshimura, K. Kosuge, H. Mitamura, T. Goto, J. Phys. Soc. Jpn. 66 (1997) 1607.

[21] H. Fjellvåg, E. Gulbrandsen, S. Aasland, A. Olsen, B.C. Hauback, J. Solid State Chem. 124 (1996) 190.